

Picking up Soft 3D Objects with Two Fingers

Huan Lin Feng Guo Feifei Wang Yan-Bin Jia

Department of Computer Science

Iowa State University

Ames, IA 50011, USA

linhuan, fguo, wangff, jia@iastate.edu

Abstract—This paper describes a simple strategy for a robot hand to grasp and lift a deformable 3D object resting on a table. Inspired by the human hand grasping, the strategy employs two rigid hemispherical fingers to first squeeze the object until a secure grip is achieved under contact friction, and then translate vertically upward. During the squeeze, a lift test is repeatedly conducted to determine if the maximum hypothetical liftable weight of the object reaches its real weight. Actual lifting follows when the test is passed. The object's deformation and configuration of contact with the fingers and the plane are tracked using the finite element method (FEM) in an event-driven manner, based on varying contact displacements induced by the finger movements. The gravitational force acting on the object is accounted for. Slips inside the contact regions are determined from solving quadratic systems. Experiment has been conducted to demonstrate the efficiency and accuracy for this sensorless grasping approach.

I. INTRODUCTION

The human hand is experienced at handling soft objects in the daily life. To pick up such an object from the table, for instance, the hand usually squeezes it first with two or more fingers to achieve a firm grip, leveraging the table's support to ensure stability. The hand starts to lift the object at some point. During the lift, as an increasing portion of the object's weight is felt, the hand may apply some extra squeeze to prevent slips.

Inspired by the human hand grasping, in this paper we introduce a simple strategy for a robotic hand with no use of tactile sensing to pick up 3D deformable objects. Two rigid fingers squeeze an object, and after every extra amount of squeeze, they perform a quick test (free of physical action) to check if the object can be lifted. Once the test is passed, the fingers stop squeezing to pick up the object via an upward translation. Throughout the process, the object is constrained by the fingers, with or without the supporting table.

Our recent work [8], [10] investigated squeeze grasping of deformable 2D objects as well as some optimal squeezing strategies. One of the ideas, reflecting a key difference from rigid body grasping, was to specify finger movements rather than finger forces. This is because force and torque equilibria are guaranteed over a deforming body that is fully constrained, following the elasticity theory [5], [3]. Another idea was to update deformation in an event-based manner during the physical action.

Grasping deformable 3D objects differs from the 2D version of the task in several aspects beyond just adding one more dimension. Gravity can no longer be ignored given the

volume (and thus the weight) of a 3D object. First, it directly affects the shape of the object as it rests on the supporting surface. Second, when the object is being lifted, complex interactions take place in the contact regions inside which every contact could slide in a continuum of directions.

Like our handling of the 2D grasping task before, we will sequence the entire operation into periods within each of which the contact configuration under a finite element discretization does not change. During a single period, the displacements of the contact nodes are either known or estimable from the finger movements. From them we can uniquely determine the object's deformation, which in turn causes new change in the contact configuration to begin the next period. A finite element analysis based on the linear elasticity theory will be given in Section II, extending the 2D result from [8].

Section III will focus on the design of the aforementioned pickup strategy. We will offer an iterative procedure to compute the object's initial deformation as it rests on a table, determining the region of support. Then, we will present a lift test to be carried out simultaneously during the squeeze of the object by two fingertips. Modeling of the object deformation and the contact configuration during the action will generalize over three-finger squeezing in 2D [10].

Section IV will describe our simulation and experiment on four different objects in real life to validate the pick-up strategy, in an effort to demonstrate accuracy and efficiency of the approach.

In this paper, we assume that the entire operation causes small deformations of the object which can be described within the scope of linear elasticity. Units from the metric system will be used.

To constrain the object from any rigid body movement, the initial finger placement needs to be force closure [13] on a rigid body assuming exactly the object's resting shape. For literature on rigid body grasping, we refer to the survey [2]. On deformable body grasping, much less effort [16], [9], [7] is known.

Within the framework of finite element method (FEM), the problem of elastic contact with friction had iterative solutions [14], [4] which updated the contact zone and the modes of individual nodes. Our handling of contact has a similar event-driven flavor but takes as input contact displacements for deformation update rather than loads under some imposed constraints that are not always realizable.

II. DEFORMED SHAPE UNDER CONTACT

This section will begin with a brief review of linear elasticity for 3D solids, and a characterization of all displacement fields that represent rigid body transformations. It will then describe an FEM formulation of deformation under gravity and external loads. It will end with solution of the deformed shape of a solid from specified contact displacements, to prepare for a grasping strategy to be detailed in Section III.

A. Linear Elasticity

Consider a 3D solid under a displacement field $(u(x, y, z), v(x, y, z), w(x, y, z))^T$. Every point $(x, y, z)^T$ inside the object moves to $(x + u, y + v, z + w)^T$. Denote by $\epsilon_x, \epsilon_y, \epsilon_z$ the normal strains along the x -, y -, and z -directions, respectively, and $\gamma_{xy}, \gamma_{xz}, \gamma_{yz}$ the shear strains in the xy -, xz -, and yz -planes, respectively. They are given below:

$$\begin{aligned} \epsilon_x &= \frac{\partial u}{\partial x}, & \epsilon_y &= \frac{\partial v}{\partial y}, & \epsilon_z &= \frac{\partial w}{\partial z}, \\ \gamma_{xy} &= \frac{\partial v}{\partial x} + \frac{\partial u}{\partial y}, & \gamma_{xz} &= \frac{\partial w}{\partial x} + \frac{\partial u}{\partial z}, & \gamma_{yz} &= \frac{\partial w}{\partial y} + \frac{\partial v}{\partial z}. \end{aligned} \quad (1)$$

The object's strain energy [5, p. 302] has the form

$$U = \frac{E}{2(1+\nu)} \int_V \left[(\epsilon_x^2 + \epsilon_y^2 + \epsilon_z^2) + \frac{\nu}{1-2\nu} (\epsilon_x + \epsilon_y + \epsilon_z)^2 + \frac{1}{2} (\gamma_{xy}^2 + \gamma_{xz}^2 + \gamma_{yz}^2) \right] dV, \quad (2)$$

where E and ν are Young's modulus and Poisson's ratio of the material, respectively, with $E > 0$ and $-1 < \nu < \frac{1}{2}$ for most materials including those considered for grasping.

Theorem 1: Under linear elasticity, any displacement field $(u, v, w)^T$ that yields zero strain energy is linearly spanned by the following six fields: $(1, 0, 0)^T$, $(0, 1, 0)^T$, $(0, 0, 1)^T$, $(0, -z, y)^T$, $(z, 0, -x)^T$, $(-y, x, 0)^T$.

Proof: (Sketch) Suppose $U = 0$. First, using (2) we can establish the vanishing of all strains, i.e., $\epsilon_x = \epsilon_y = \epsilon_z = \gamma_{xy} = \gamma_{xz} = \gamma_{yz} = 0$. Substitution of (1) into the above yields six partial differential equations (PDEs) with zeros on the right hand sides. Integration of the first three yields $u = u(y, z)$, $v = v(x, z)$, $w = w(x, y)$. Plug them and (1) into the last three PDEs for integration. We obtain two equivalent forms for each of u, v, w . Further reasoning over the equivalences will lead to

$$\begin{pmatrix} u \\ v \\ w \end{pmatrix} = \rho_1 \begin{pmatrix} 0 \\ -z \\ y \end{pmatrix} + \rho_2 \begin{pmatrix} z \\ 0 \\ -x \end{pmatrix} + \rho_3 \begin{pmatrix} -y \\ x \\ 0 \end{pmatrix} + \begin{pmatrix} \rho_4 \\ \rho_5 \\ \rho_6 \end{pmatrix},$$

for some constants ρ_1, \dots, ρ_6 . Hence the conclusion. ■

The first three displacement fields in the theorem represent unit translations in the x -, y -, and z -directions, respectively. The next three fields represent rotations about the x -, y , and z -axes under linear elasticity, respectively.

B. The Finite Element Method with Gravity

For convenience, we assume that the object has uniform mass density, and set the origin at its center of mass. The FEM [6] is applied to evaluate the strain energy (2), which generally has no closed form. Represent the solid as a tetrahedral mesh with n vertices $\mathbf{p}_1, \dots, \mathbf{p}_n$, where $\mathbf{p}_i =$

$(x_i, y_i, z_i)^T$, for $1 \leq i \leq n$. When the body deforms, every node \mathbf{p}_k is displaced by δ_k to the location $\tilde{\mathbf{p}}_k = \mathbf{p}_k + \delta_k$. Inside a tetrahedron, the displacement of a point is linearly interpolated over those of the four vertices. The deformed shape is thus described by $\Delta = (\delta_1^T, \dots, \delta_n^T)^T$, referred to as the *displacement vector*. The total strain energy takes the form $U = \frac{1}{2} \Delta^T K \Delta$, where the $3n \times 3n$ matrix K is referred to as the *stiffness matrix*. Let $\mathbf{F} = (\mathbf{f}_1^T, \dots, \mathbf{f}_n^T)^T$ be the vector of the external forces applied at the n nodes.

We can infer from Theorem 1 that the stiffness matrix has a null space spanned by six $3n$ -vectors: $\mathbf{t}_x, \mathbf{t}_y, \mathbf{t}_z, \mathbf{r}_x, \mathbf{r}_y$, and \mathbf{r}_z . The first three vectors describe unit translations of all nodes along the x -, y -, and z -directions, respectively. The next three displace every node $(x_i, y_i, z_i)^T$ by $(0, -z_i, y_i)^T$, $(z_i, 0, -x_i)^T$, and $(-y_i, x_i, 0)^T$, respectively.

On the 3D solid, the gravitational force can rarely be ignored. Under uniform mass distribution, every element has mass proportional to its volume. We charge the element's mass evenly to its four vertices. Let the vector \mathbf{G} gather all nodal gravitational forces. It is easy to verify that \mathbf{G} is orthogonal to $\mathbf{t}_x, \mathbf{t}_y, \mathbf{r}_x, \mathbf{r}_y, \mathbf{r}_z$ but not \mathbf{t}_z , with which it has a dot product $-mg$, where m is the object's mass and $g = 9.8$ is the gravitational acceleration.

The potential energy of the system is $\frac{1}{2} \Delta^T K \Delta - \Delta^T (\mathbf{F} + \mathbf{G})$. At equilibrium, it reaches the minimum value with $K \Delta = \mathbf{F} + \mathbf{G}$.

The stiffness matrix K is symmetric and positive semidefinite. The matrix has a spectral decomposition [15, p. 273] $K = V \Lambda V^T$, where $V = (\mathbf{v}_1, \dots, \mathbf{v}_{3n})$ and $\Lambda = \text{diag}(\lambda_1, \dots, \lambda_{3n-6}, 0, \dots, 0)$. Here $\lambda_1, \dots, \lambda_{3n-6}$ are positive eigenvalues corresponding to the unit eigenvectors $\mathbf{v}_1, \dots, \mathbf{v}_{3n-6}$. The unit eigenvectors $\mathbf{v}_{3n-5}, \dots, \mathbf{v}_{3n}$ are orthogonalized over $\mathbf{t}_x, \mathbf{t}_y, \mathbf{t}_z, \mathbf{r}_x, \mathbf{r}_y, \mathbf{r}_z$ using the Gram-Schmidt procedure.

Due to the singularity of K , boundary conditions are needed to solve $K \Delta = \mathbf{F} + \mathbf{G}$. They will come from the displacements of the contact nodes with the squeezing fingers and the supporting plane.

C. Deformation from Specified Contact Displacements

The set of contact nodes will not vary during a very small period of squeeze on the solid by the fingers. As in our recent work [8] on grasping 2D objects, the starting point of modeling is to compute the deformation of the 3D object from specified displacements $\delta_{i1}, \dots, \delta_{im}$ of some boundary nodes $\mathbf{p}_{i1}, \dots, \mathbf{p}_{im}$, which are supposed to be in contact with the grasping fingers or the supporting plane. We refer to the set $\mathbb{C} = \{i_1, \dots, i_m\}$ as the *contact index set*. Zero external forces are applied at the non-contact nodes, that is, $\mathbf{f}_k = 0$, for $k = 1, \dots, 2n$ and $k \notin \mathbb{C}$.

Denote by $\bar{\mathbf{a}}$ the vector that selects the entries from a $3n$ -vector \mathbf{a} indexed at $3i_1 - 2, 3i_1 - 1, 3i_1, \dots, 3i_m$ that correspond to $\mathbf{p}_{i1}, \dots, \mathbf{p}_{im}$. For instance, $\bar{\Delta} = (\delta_{i1}^T, \dots, \delta_{im}^T)^T$, which is referred to as the *contact displacement vector*.

We can solve for the contact force vector $\bar{\mathbf{F}}$ and the displacement field Δ from $\bar{\Delta}$ by performing a procedure similar to the one in [8]. Substitute $K = V \Lambda V^T$ into

$K\Delta = F + G$, and left multiply both sides of the resulting equation with V^T . This yields the projections of Δ onto v_1, \dots, v_{3n-6} . Let the 6-vector b gather the projections of Δ onto the v_{3n-5}, \dots, v_{3n} . We reconstruct Δ in terms of v_1, \dots, v_{3n} and b . Next, extract from Δ the expressions for $\delta_{i1}, \dots, \delta_{im}$, and combine them with the six equations $v_k^T(F + G) = v_k^T K\Delta = 0$, $k = 3n - 5, \dots, 3n$. Substitute $v_k^T F = \bar{v}_k^T \bar{F}$ and introduce the constant vector $D = \sum_{k=1}^{3n-6} \frac{1}{\lambda_k} (v_k^T G) v_k$. This finally leads to a matrix equation in terms of \bar{F} and b as below:

$$\begin{pmatrix} A & B \\ B^T & 0 \end{pmatrix} \begin{pmatrix} \bar{F} \\ b \end{pmatrix} = \begin{pmatrix} \bar{\Delta} - \bar{D} \\ (0, 0, mg/\sqrt{n}, 0, 0, 0)^T \end{pmatrix}, \quad (3)$$

where the $3m \times 3m$ matrix $A = \sum_{k=1}^{3n-6} \frac{1}{\lambda_k} \bar{v}_k \bar{v}_k^T$ and the $3m \times 6$ matrix $B = (\bar{v}_{3n-5}, \dots, \bar{v}_{3n})$. Denote by M the square matrix on the left hand side in (3). In the above process, the displacement vector can be written as

$$\Delta = \sum_{k=1}^{3n-6} \frac{1}{\lambda_k} (\bar{v}_k^T \bar{F}) v_k + (v_{3n-5}, \dots, v_{3n}) b + D. \quad (4)$$

When $m = 1, 2$, we can easily show that B is singular. The singularity of M immediately follows from that its last six rows $(B^T, 0)$ are linearly dependent.

Proposition 2: $\text{rank}(B) = 6$ when $m \geq 3$ if and only if the contacts are non-collinear.

Proof: (Sketch) Note that the column space $\text{col}(B)$ of B is the same as that of the matrix $Q = (\bar{t}_x, \bar{t}_y, \bar{t}_z, \bar{r}_x, \bar{r}_y, \bar{r}_z)$. Thus, $\text{rank}(B) = \text{rank}(Q)$.

We first focus on the case of three distinct contact points p_i, p_j, p_k . To determine the rank of the 9×6 matrix Q , for $l = 1, 2, 3$ we subtract row l from rows $l + 3$ and $l + 6$. In the resulting matrix, the first three columns contain the 3×3 identity matrix at the top and zero entries below. We can show that, when p_i, p_j , and p_k are collinear, rows 7 to 9 are scaled by the same factor from rows 4 to 6 (which are linearly independent themselves), respectively. This implies that Q and B all have rank 5 when the three points are collinear. The conclusion generalizes easily to $m > 3$ contacts in that $\text{rank}(B) = 5$ when p_{i_1}, \dots, p_{i_m} are collinear. Geometrically, the object is free to rotate about the line through these points.

If p_i, p_j and p_k are not collinear, we can establish that the matrix $\begin{pmatrix} Q_2 \\ Q_3 \end{pmatrix}$ has rank 3 via subtractions of (scaled) rows and reasoning under the assumption $x_i \neq x_j$, without loss of generality, over whether $(x_j - x_i, y_j - y_i)$ and $(x_k - x_i, y_k - y_i)$ are in the same direction. ■

Collinearity of all the m contacts implies singularity of B and thus of M . When the m contacts are not collinear, by a reasoning similar to that in [8], we can show that $M(\bar{F}^T, b^T)^T \neq 0$ if $\bar{F} \neq 0$ or $b \neq 0$.

Theorem 3: The matrix M is non-singular if and only if the m contact points are not collinear.

Therefore, when the $m \geq 3$ contacts are not collinear, the system (3) has a unique solution; in other words, the deformation is uniquely determined. We multiply both sides

Algorithm 1 Two-finger pickup of a 3D solid

Input: tetrahedral mesh, table contact $\Delta p_q p_r p_s$, finger contacts p_i, p_j , squeeze $(\hat{d}_1, \hat{s}d_2)$

- 1: Check if p_i and p_j form force closure with $\Delta p_q p_r p_s$. If not, return failure.
 - 2: Compute the object's initial resting configuration.
 - 3: Squeeze the object by translating \mathcal{F}_1 and \mathcal{F}_2 .
 - 4: During the squeeze, test if the object can be lifted.
 - 5: If so, stop squeezing to lift the object. Return success.
 - 6: If enough squeeze has been applied and the object still cannot be picked up, report failure. Otherwise, go back to step 3.
-

of (3) with M^{-1} , obtaining b and

$$\bar{F} = C(\bar{\Delta} - \bar{D}) + \frac{mg}{\sqrt{n}} e, \quad (5)$$

where C is a matrix of dimension $3m \times 3m$ referred to as the *reduced stiffness matrix* [10], and e is some vector. The equation relates the contact forces to the specified contact displacements. With \bar{F} and b determined, the displacement vector follows from (4).

III. GRASPING TO PICK UP A SOLID

Having studied deformation under contact, we move on to consider the task of using two fingers to pick up a deformable 3D solid on a table, which is a (horizontal) plane \mathcal{P} . The object's initial resting configuration is determined from a surface triangle $\Delta p_q p_r p_s$ in contact with \mathcal{P} . The vertical projection of the object's center of mass lies in the interior of the triangle. The object deforms under gravity over the triangle, causing the contact region to grow from $\Delta p_q p_r p_s$.

The fingers have identical hemispherical tips \mathcal{F}_1 and \mathcal{F}_2 for simplicity. Making contact with the resting object at the nodes p_i and p_j in their current locations under gravity, the fingertips first squeeze the object and later lift it via an upward translation, breaking its contact with the plane.

In the current state of our work, the fingers are assumed to be translating during the squeeze in constant directions, denoted by unit vectors \hat{d}_1 and \hat{d}_2 , respectively. Without loss of generality, let \mathcal{F}_1 be the moving fingertip. For every unit distance \mathcal{F}_1 translates in \hat{d}_1 , \mathcal{F}_2 translates in \hat{d}_2 by $s \geq 0$. Thus, the squeeze action can be represented by $\rho(\hat{d}_1, \hat{s}d_2)$, where $\rho \geq 0$ is referred to as the *squeeze depth*.

As ρ increases, the contacts will grow from p_i and p_j into regions on the fingertips. The contact region with the plane will also change and later shrink during the lift. Denote by $\mathbb{I}, \mathbb{J}, \mathbb{K}$ the (varying) sets of the indices of the nodes that are in contact with $\mathcal{F}_1, \mathcal{F}_2, \mathcal{P}$, respectively. Their union $\mathbb{C} = \mathbb{I} \cup \mathbb{J} \cup \mathbb{K}$ consists of the indices of all contact nodes.

Algorithm 1 describes how to pick up the object. Step 1 uses a procedure from [11] to check if p_i, p_j , and the center of $\Delta p_q p_r p_s$ would be force closure on a rigid body with the same shape of the resting object.¹ If no force closure, the object will not deform and the algorithm will fail.

¹Since the triangle is small, the contact is approximated by its center.

Below we will first describe step 2 on modeling of the object's resting configuration (when it is in contact with \mathcal{P} only), then step 4 on testing whether the object can be lifted after some squeeze (by considering its contacts with \mathcal{F}_1 and \mathcal{F}_2 only), and finally step 3 on squeezing the object (when it has active contacts with all of \mathcal{F}_1 , \mathcal{F}_2 , and \mathcal{P}).

A. Initial Resting Configuration

Before grasping the object, we need to estimate its resting configuration on the table. Clearly, $\mathbb{I} = \mathbb{J} = \emptyset$ and $\mathbb{C} = \mathbb{K}$ since the object has not yet made contact with the fingertips.

We describe an iterative procedure that computes the initial resting configuration. At the start of each iteration, a node \mathbf{p}_k , $1 \leq k \leq n$, has been displaced to the location $\tilde{\mathbf{p}}_k$ and receives force \mathbf{f}_k if it is in contact with the plane. Let the set \mathbb{P} collect the indices of sliding nodes. The following steps are carried out in the iteration.

- 1: $\mathbb{P} \leftarrow \emptyset$.
- 2: Compute the change Δ' from displacement vector Δ , and the change $\bar{\mathbf{F}}'$ from contact force vector $\bar{\mathbf{F}}$.
- 3: $\Delta \leftarrow \Delta + \Delta'$ and $\bar{\mathbf{F}} \leftarrow \bar{\mathbf{F}} + \bar{\mathbf{F}}'$.
- 4: If no new contact node is found and, for every $k \in \mathbb{K}$, \mathbf{f}_k is inside the friction cone, terminate the algorithm.
- 5: Otherwise, handle new contact if any.
- 6: Identify sliding nodes and add their indices to \mathbb{P} .
- 7: Recompute the displacements of all sliding nodes.

In step 2, we fix every contact node \mathbf{p}_k at $\tilde{\mathbf{p}}_k$, $k \in \mathbb{C}$, by setting its change in displacement $\delta'_k \leftarrow 0$. The change Δ' in the contact displacement vector, which consists of all δ'_k , $k \in \mathbb{C}$, is thus zero. Evaluate $\bar{\mathbf{F}}'$ and Δ' according to (5) and (4) after substitutions of Δ' , $\bar{\mathbf{F}}'$, $\bar{\Delta}'$ for Δ , $\bar{\mathbf{F}}$, $\bar{\Delta}$, respectively. Set $\tilde{\mathbf{p}}_k \leftarrow \tilde{\mathbf{p}}_k + \delta'_k$, for $1 \leq k \leq n$, as described in step 3.

In step 4, a new contact exists if some node on the object would be displaced below the plane. Among all such nodes, let \mathbf{p}_t be the one that is the furthestmost below \mathcal{P} . Step 5 adds \mathbf{p}_t as the new contact; namely, $\mathbb{C} \leftarrow \mathbb{C} \cup \{t\}$, and scale down δ'_t such that $\tilde{\mathbf{p}}_t + \delta'_t$ lies in \mathcal{P} .

Step 6 determines if any existing contact \mathbf{p}_k , $k \in \mathbb{C}$ and $k \neq t$, has slid by checking if \mathbf{f}_k is outside the friction cone. If the condition holds, add k to \mathbb{P} . The sliding direction of a sliding node is opposite to the projection of \mathbf{f}_k onto the plane. The extra displacement δ'_k due to sliding is thus determined by the sliding distance d_k .

Step 7 evaluates $\bar{\mathbf{F}}'$ and Δ' again as in step 2, this time from the updated δ'_k for $k \in \mathbb{P}$, δ'_t , and $\delta'_l = 0$ for $l \in \mathbb{C} \setminus (\mathbb{P} \cup \{t\})$. Each updated \mathbf{f}_k , $k \in \mathbb{P}$, is a linear function of d_l for all $l \in \mathbb{P}$. That \mathbf{f}_k is on the boundary of the friction cone yields a system of quadratic equations:

$$(1 + \mu_{\mathcal{P}}^2)(\mathbf{f}_k \cdot \hat{\mathbf{z}})^2 = \mathbf{f}_k \cdot \mathbf{f}_k, \quad \text{for } k \in \mathbb{P}, \quad (6)$$

where $\mu_{\mathcal{P}}$ is the coefficient of friction between the object and the table. There are $|\mathbb{P}|$ equations in $|\mathbb{P}|$ variables d_k , $k \in \mathbb{P}$. Solve the system using the homotopy continuation

method² [1]. Move on to the next iteration.

B. Lift Test

When the squeeze depth is small, the friction between the object and the two fingertips is not enough to hold the object if it is picked up. We need to perform a quick lift test in order to check if the object can be picked up. This corresponds to step 4 in Algorithm 1.

A straight forward strategy is to approximate the deformation after the lift in one shot. We first set $\mathbb{C} \leftarrow \mathbb{I} \cup \mathbb{J}$, as if the supporting plane \mathcal{P} were suddenly removed. Then, the contact force vector and the displacement field are recomputed by specifying the displacements of only the nodes in contact with the fingertips. Finally, we identify the sliding nodes. If some finger slides or the portion of the sliding nodes is beyond some threshold, we consider the test as a failure.

However, dramatic change in the contact set from $\mathbb{C} \leftarrow \mathbb{I} \cup \mathbb{J} \cup K$ and the corresponding constraints will make it almost impossible to keep track of the sliding distances. We need a strategy that could preserve the incremental nature and still be interleaved with the squeezing action well.

Imagine we hypothetically increase the weight of the object from zero. Beyond certain value w , one finger will slide on the object. We call w as *liftable weight*. Here we assume that w increases continuously with the squeeze depth ρ . As the squeeze goes on and ρ increases, we keep track of $w(\rho)$. Initially, $w(0) = 0$. At each step l update $w(\rho_l)$ based on the current contact configuration and $w(\rho_{l-1})$. We iterate to test $w(\rho_{l-1}) + h$, $w(\rho_{l-1}) + 2h$, ..., until the object is no longer liftable at some $w(\rho_{l-1}) + kh$, where h is the step size. Set $w(\rho_l) = w(\rho_{l-1}) + (k-1)h$. Once w reaches or exceeds the actual weight of the object, the lift test is passed. Otherwise, more squeeze is needed. And the lift test fails.

Since the test is repeated for every small increment in ρ , small change takes place which avoids the loss of tracking sliding distance.

C. Squeezing and Lifting the Object

In step 3 of Algorithm 1, the object is being squeezed by \mathcal{F}_1 and \mathcal{F}_2 under translations $\rho\hat{\mathbf{d}}_1$ and $\rho\hat{\mathbf{d}}_2$, respectively, with ρ increasing. The squeeze continues until either at some instant the lift test is passed, or the amount of squeeze becomes too large that the object is deemed impossible to pick up under the initial finger placement and squeezing directions.

We here generalize the three-finger squeeze algorithm for 2D deformable objects from our recent work [10]. Sequence ρ into $\rho_0 = 0 < \rho_1 < \dots$ such that at $\rho = \rho_l$ some event happens to trigger a change in the contact configuration. Within

²This method solves a system $\mathbf{P}(\mathbf{x}) = 0$ by tracking the solutions of "nearby" systems starting with another system $\mathbf{Q}(\mathbf{x}) = 0$ that has a known solution. For instance, the `RootFinding[Homotopy]` function [12] of the mathematics software Maple constructs a system $\mathbf{H}(\mathbf{x}, t) = (1 - (1 - t)^2)\mathbf{P}(\mathbf{x}) + (1 - t)^2\mathbf{Q}(\mathbf{x})$, $t \in [0, 1]$, such that $\mathbf{H}(\mathbf{x}, 0) = \mathbf{Q}(\mathbf{x})$ and $\mathbf{H}(\mathbf{x}, 1) = \mathbf{P}(\mathbf{x})$. It tracks the solution by varying t from 0 to 1 via numerical integration over the derivative of $d\mathbf{H}/dt$, and polishes the root estimate \mathbf{x} after the integration step at each t value using Newton's method.

the interval $[\rho_l, \rho_{l+1})$ the changes $\bar{\mathbf{F}}'$ in the contact forces and $\bar{\Delta}'$ in the displacement vector are updated according to the modified (5) and (4).

There are four events: contact establishment (A), contact break (B), stick-to-slip (C), and slip-to-stick (D). The contact index sets $\mathbb{I}, \mathbb{J}, \mathbb{K}$ do not change until the next event. Event A is detected when a node is to penetrate into $\mathcal{F}_1, \mathcal{F}_2$, or \mathcal{P} . Event B happens when the contact force at a node is pointing outward from the object. Event C takes place when the contact force at a node is out of its friction cone. Event D occurs when the change rate of the sliding distance of some node in terms of ρ becomes zero.

Between two events, the movements of all sliding nodes need to be tracked. Their indices are collected in the set \mathbb{P} . If p_k slides in the plane \mathcal{P} , its sliding distance d_k is a variable as described in Section III-A.

The situation that p_k slides on a fingertip is illustrated in Fig. 1. Let \tilde{p}_k be its current position before the slip, and

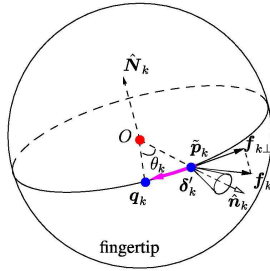


Fig. 1. Sliding of a node on a hemispherical fingertip (with the entire sphere shown).

δ'_k the extra displacement due to the slip. Let \hat{n}_k be the normal at \tilde{p}_k pointing into the object. The contact force \mathbf{f}_k , out of the friction cone at \tilde{p}_k , has a tangential component $\mathbf{f}_{i\perp} = \mathbf{f}_k - (\mathbf{f}_k \cdot \hat{n}_k)\hat{n}_k$. We assert that the node p_k will slide from its current position \tilde{p}_k in the opposite direction of $\mathbf{f}_{k\perp}$ and reach some point q_k on the great circle coplanar with $\mathbf{f}_{k\perp}$ and \hat{n}_k . Namely, $\delta'_k = q_k - \tilde{p}_k$.

The unit normal \hat{N}_k to the plane containing this great circle is in the direction of $\hat{n}_k \times \mathbf{f}_{i\perp}$. Thus, q_k is obtained from rotating \tilde{p}_k about \hat{N}_k through some angle $\theta_k < 0$. We obtain $q_k = O + c_k(\tilde{p}_k - O) + s_k(\hat{N}_k \times (\tilde{p}_k - O))$, where c_k and s_k are the shorthand notations for $\cos \theta_k$ and $\sin \theta_k$, respectively. Coulomb's law of friction induces a quadratic equation:

$$(1 + \mu_{\mathcal{F}}^2)(\mathbf{f}_k \cdot \hat{n}_k)^2 = \mathbf{f}_k \cdot \mathbf{f}_k, \quad (7)$$

coupled with

$$c_k^2 + s_k^2 = 1. \quad (8)$$

In the above, $\mu_{\mathcal{F}}$ is the coefficient of friction between the object and a fingertip.

With the updated δ'_k s, whether p_k slides in the plane or on a fingertip, the change $\bar{\Delta}'$ in the contact displacement vector has been reset. We can obtain the changes $\bar{\Delta}'$ in the displacement vector and $\bar{\mathbf{F}}'$ in the contact force according to (4) and (5) after substitutions of $\bar{\Delta}', \bar{\mathbf{F}}'$ for $\Delta, \mathbf{F}, \bar{\Delta}$. They depend on all $d_k, k \in \mathbb{P} \cap \mathbb{K}$, and all c_l and $s_l, l \in$

$\mathbb{P} \cap (\mathbb{I} \cup \mathbb{J})$. We end up with a system of $2|\mathbb{P} \cap (\mathbb{I} \cup \mathbb{J})| + |\mathbb{P} \cap \mathbb{K}|$ quadratic equations in the forms of (6), (7), or (8) in the same number of variables. Solve the system to update all contact slips using the homotopy continuation method.

Instead of combining the above system with the condition for each event test to determine the next squeeze depth at which an event happens, we take small increments in the squeeze depth and check after each increment if any event happens. Upon such an occurrence, we can use Newton's method to polish the corresponding squeeze depth value. The contact index sets $\mathbb{I}, \mathbb{J}, \mathbb{K}, \mathbb{P}$ are updated accordingly.

In step 5 of Algorithm 1, once the lift test is passed, the two fingers translate upward. During the lift, the nodal contacts with the plane \mathcal{P} will break gradually, and some contacts with the fingertips could also break under gravity. Modeling, however, is no different from that of squeezing. If all the contact nodes on one finger are sliding, the object slides on the finger and the pickup fails. Otherwise, the pickup is a success when the object leaves the plane.

IV. SIMULATION AND EXPERIMENT

Simulation was done on a PC with Intel Core i7-3770 Processors and 8 GB system RAM. Experiment was carried out to validate Algorithm 1. A triangular mesh for every object used in the experiment was first acquired by a 3D scanner from Next Engine, Inc., and then simplified using MeshLab (<http://meshlab.sourceforge.net/>). The generation of tetrahedral meshes and transformation of the objects were implemented using Computation Geometry Algorithm Library (<http://www.cgal.org>).

Table I listed the parameters of four deformable objects, shown in the first row of Table II, which were used in experiment: w is the weight of the object, E is the Young's modulus, ν is the Poisson's ratio, and μ is the coefficient of friction.

	tomato	orange	steam bun	football
# vertices	490	600	658	875
# surface facets	498	564	646	782
# tetrahedra	2129	2692	2941	4058
w	1.246	1.868	0.467	0.489
E	1.0×10^5	1.4×10^5	2×10^3	6×10^3
ν	0.4	0.4	0.2	0.3
μ	0.32	0.34	0.4	0.5

TABLE I
PARAMETERS OF OBJECTS USED IN EXPERIMENT.

Table II shows successful pickups of four objects. The second row displays their tetrahedral mesh representations. Two fingers of Barrett Hand equipped with hemispherical fingertips made initial contacts with the object. Then the two fingertips applied a squeeze by $(\hat{d}_1, s\hat{d}_2)$, where $\hat{d}_1 = (0, 0.974, -0.227)$, $\hat{d}_2 = (0, -0.974, -0.227)$, and $s = 1$. Once the liftable weight determined by lift test exceeded the weight of the object, the fingers switched the action to lifting. The third row shows the four objects picked up by the Barrett Hand driven by Algorithm 1. The fourth row

shows the corresponding simulation results. The last row lists the relevant values: number of contact nodes in the final configuration, squeeze depth ρ before lifting, and running time(s) of the simulation for prediction.





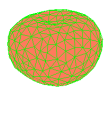
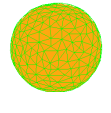
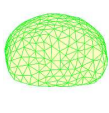
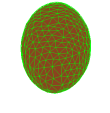




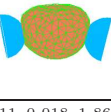
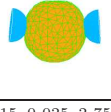
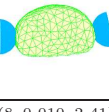
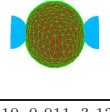
			
			
			
			
(11, 0.018, 1.86)	(15, 0.025, 2.75)	(8, 0.010, 2.41)	(10, 0.011, 3.12)

TABLE II

SUCCESSFUL PICKUPS OF FOUR DEFORMABLE OBJECTS. INITIAL RESTING CONFIGURATIONS IN EXPERIMENT (ROW 1) AND FROM SIMULATION (ROW 2). THE FINAL CONFIGURATIONS OF GRASPING IN EXPERIMENT (ROW 3) AND SIMULATION (ROW 4). NUMBER OF CONTACT NODES, SQUEEZE DEPTH, RUNNING TIME (ROW 5).

Also, we compared the grasping results with those of grasping four rigid bodies that have identical shapes of the four objects in Table II. Table III shows the total normal force needed to balance the gravity and pick up an object in both cases. The comparison shows that picking up deformable objects takes less effort than rigid bodies. This is mainly because that smaller normal force is needed to generate enough friction for deformable objects due to increased contact area under deformation.

V. DISCUSSION AND FUTURE WORK

We have described a simple squeeze-and-lift strategy for grasping 3D deformable objects. The idea is to model changes in shape and contact geometry during the action, and repeatedly conduct lift tests to predict when to switch the action from squeezing to lifting. To support the modeling,

	tomato	orange	steam bun	football
deformable	2.68	4.35	1.01	0.96
rigid	2.96	4.82	1.16	1.09

TABLE III

PICK-UP COMPARISON FOR DEFORMABLE AND RIGID OBJECTS WITH THE SAME SHAPES IN EXPERIMENT.

we have extended our contact-based finite element analysis to 3D, with gravity taken into account. Contact slips are handled via root finding of quadratic systems derived under Coulomb's friction law and linear elasticity.

The next step is to obtain more understanding about several factors that contribute to a successful pickup: global shape, geometry of contact regions, normal vs. tangential contact forces in balancing the object's weight, etc. Experiment on same shape with different softness and objects with complex geometry will be conducted.

In the near future, our efforts will be on optimizing finger placements and squeezing directions, and turning the operation into a reactive one by incorporating tactile data in the modeling for reliable slip detection/prediction.

VI. ACKNOWLEDGMENT

Support for this research was provided in part by Iowa State University (ISU), and in part by the National Science Foundation through the grant IIS-0915876. Any opinions, findings, and conclusions or recommendations expressed in this material are those of the author(s) and do not necessarily reflect the views of the National Science Foundation. The authors are grateful to the anonymous reviewers for their valuable and constructive feedback.

REFERENCES

- [1] E. L. Allgower and K. Georg, "Numerical path following," in *Handbook of Numerical Analysis*, vol. 5, North-Holland, 1997.
- [2] A. Bicchi and V. Kumar, "Robotic grasping and contact: a review," in *Proc. IEEE Intl. Conf. Robot. Autom.*, 2000, pp. 348–353.
- [3] A. F. Bower, *Applied Mechanics of Solids*, CRC Press, Boca Raton, Florida, 2009.
- [4] N. Chandrasekaran, W. E. Haisler, and R. E. Goforth, "A finite element solution method for contact problems with friction," *Int. J. Num. Meth. Engr.*, vol. 24, pp. 477–495, 1987.
- [5] S. H. Crandall, N. C. Dahl and T. J. Lardner, *An Introduction to the Mechanics of Solids*, 2nd edition, McGraw-Hill, 1978.
- [6] R. H. Gallagher, *Finite Element Analysis: Fundamentals*, Prentice-Hall, Englewood Cliffs, N.J., 1975.
- [7] K. Gopalakrishnan and K. Goldberg, "D-space and deform closure grasps of deformable parts," *Int. J. Robot. Res.*, vol. 24, pp. 899–910, 2005.
- [8] F. Guo, H. Lin, and Y.-B. Jia, "Squeeze grasping of deformable planar objects with segment contact and stick/slip transitions," in *Proc. IEEE Intl. Conf. Robot. Autom.*, 2013, pp. 3721–3726.
- [9] S. Hirai, T. Tsuboi, and T. Wada, "Robust grasping manipulation of deformable objects," in *Proc. IEEE Symp. Assembly and Task Planning*, 2001, pp. 411–416.
- [10] Y.-B. Jia, H. Lin, and F. Guo, "Optimal two-finger squeezing of deformable object," in *Proc. IEEE/RSJ Intl. Conf. Intell. Robots and Systems*, 2013, pp. 3514–3519.
- [11] J. W. Li, H. Liu, and H. G. Cai, "On computing three-finger force-closure grasps of 2-D and 3-D objects," *IEEE Trans. Robot. Automat.*, vol. 19, pp. 155–161, 2003.
- [12] <http://www.maplesoft.com/support/help/Maple/view.aspx?path=RootFinding/Homotopy>.
- [13] V. D. Nguyen, "Constructing force-closure grasps," *Int. J. Robot. Res.*, vol. 7, pp. 3–16, 1988.
- [14] T. D. Sachdeva and C. V. Ramakrishnan, "A finite element solution for the two-dimensional elastic contact problems with friction," *Int. J. Num. Meth. Engr.*, vol. 17, pp. 1257–1271, 1981.
- [15] Strang, G.: *Introduction to Linear Algebra*, 2nd edition, Wellesley-Cambridge Press, 1993.
- [16] H. Wakamatsu, S. Hirai and K. Iwata, "Static analysis of deformable object grasping based on bounded force closure," in *Proc. IEEE/RSJ Intl. Conf. Intell. Robots and Systems*, 1996, pp. 3324–3329.